Permafrost and Periglacial Processes

WILEY

RESEARCH ARTICLE OPEN ACCESS

Effect of Sea Water Inundation on CO_2 and CH_4 Production of Thawing Coastal Permafrost Near Utqiaġvik, Alaska

Madina Lucia Dolle[1,2] | Mélissa Laurent[1,3] | Fabian Seemann[1,3] | Jörg Schaller[4] | Maren Jenrich[1,3] | Jens Strauss[1] | Claire Treat[1,5]

[1]Permafrost Research Section, Alfred Wegener Institute Helmholtz Centre for Polar and Marine Research, Potsdam, Germany | [2]University of Geography, University of Hamburg, Hamburg, Germany | [3]Institute of Geosciences, University of Potsdam, Potsdam, Germany | [4]Leibniz-Center for Agricultural Landscape Research (ZALF), Müncheberg, Germany | [5]Center for Landscape Research in Sustainable Agricultural Futures, Aarhus University, Aarhus, Denmark

Correspondence: Mélissa Laurent (melissa.laurent@awi.de)

Received: 16 October 2024 | **Revised:** 13 August 2025 | **Accepted:** 20 August 2025

Funding: Funding for this study was provided by European Research Council Starting Grant 851181 (FluxWIN).

ABSTRACT

Rising sea levels and changing marine dynamics are increasing the inundation of previously terrestrial permafrost, accelerating thaw and altering microbial carbon cycling. On the Arctic Coastal Plain of Alaska, permafrost features like drained lake basins (DLBs) and uplands (ULs), offer distinct redox conditions and formation histories that may influence the carbon cycling response to sea water inundation. This study investigates changes in CO_2 and CH_4 production during potential seawater inundation using ex situ anaerobic incubations of soils from a DLB and a UL near Utqiaġvik, Alaska. Results showed that CO_2 and CH_4 production was, respectively, up to 2.2 and 3.3 times higher in the DLB site than in the UL site with the salt-less control treatment. The addition of artificial sea water inhibited CH_4 production at both sites. CO_2 production increased in the active and permafrost layers of the UL site, decreased in surface layers of both sites, and remained unaffected by saltwater treatments in the permafrost layers of the DLB site, likely due the presence of marine sediments in the DLB. Carbon availability, microbial adaptation, and electron acceptors are potential factors for the CO_2 and CH_4 response. Overall, the results of this study showed that anaerobic CO_2 production responded differently to sea water at different landscape positions and formation histories while CH_4 was inhibited independently of the landscape position. Those results highlight the need to consider local hydrology and landscape history in future GHG projections for coastal permafrost.

1 | Introduction

Coastal permafrost (PF) regions are highly dynamic environments at the land-ocean interface. Coastal PF areas are characterized as environments exposed to both terrestrial and marine influences and representing 34% of all global coasts [1]. Climate change impacts coastal PF at the sea site by rising sea levels, increasing open water seasons, warming and thawing PF on—and offshore. But it also has consequences on terrestrial coastal PF for example with rising coastal erosion rates and more extreme storm events [1–4]. With more frequent storm surges and sea-level rise, an increasing area of coastal PF becomes inundated and exposed to thaw. On the Arctic Coastal Plain of Alaska, the study region of this study, inundations cause shoreline retreats of up to 25 m $year^{-1}$ [5, 6]. This inundation process can represent the first step of forming a PF lagoon where long-term terrestrial PF transforms into subsea PF [7, 8].

The rapid changes in coastal PF due to climate change also affect carbon cycle [3]. PF regions store 50% of global terrestrial

Madina Lucia Dolle and Mélissa Laurent contributed equally to this work.

carbon (1460–1600 Pg terrestrial carbon in PF regions [9]). When PF thaws, organic carbon stored in PF soils is destabilized, accelerating the release of greenhouse gases (GHGs) such as carbon dioxide (CO_2) and methane (CH_4) into the atmosphere [10]. However, CO_2 and CH_4 response to climate change in these environments remain understudied [11].

In terrestrial PF soils, the release of CO_2 and CH_4 to the atmosphere is heavily affected by soil moisture and drainage [12–15]. On the Arctic Coastal Plain of Alaska, carbon cycling is closely linked to the small-scale topography which creates a heterogeneous soil environment [16, 17]. The landscape is dominated by drained thaw lake basins (DLBs) and relatively higher lying interstitial tundra [18]. At these two landscape positions, soil moisture forms two different soil environments: (1) well drained soils with prevailing aerobic conditions such as uplands (ULs) and (2) poorly drained soils with prevailing anaerobic conditions such as DLBs [19]. For carbon cycling microbes, anoxic conditions mean that oxygen is not available as electron acceptor for energy production. Thus, other electron acceptors need to be used by microbes for carbon cycling. The choice of elecetron acceptor used for the reaction depends on the redox conditions of the soil. Under anoxic conditions nitrogen is used first, then iron, followed by sulfate (SO_4^{2-}), and finally CO_2 allowing for methanogenesis [20]. Therefore CH_4 is usually produced under anaerobic conditions when all the other electron acceptor pools are depleted [20]. Under oxic conditions, oxygen is used as an electron acceptor resulting in CO_2 production [20].

Until now, most climate models do not include changes in local hydrology in GHG emission projections following PF thaw [21]. However, sea water inundations alter soil properties, promote anaerobic conditions in sediments, and facilitate the transport of labile carbon substrates from land to sea [4]. Although anoxic conditions are known to enhance CH_4 production, the increase of salinity inhibits methanogenesis [11, 22, 23]. SO_4^{2-} contained in sea water is thermodynamically more favorable and therefore will be preferentially used as electron acceptor than methanogenesis. However, a few studies have shown that in relatively newly flooded lowlands, CH_4 production can be established under brackish conditions [23]. Under aerobic conditions mimicking coastal erosion, CO_2 production was found to be increased by sea water addition, while CH_4 was produced only in neglectable amounts [4]. The increased CO_2 production was associated with sea water discriminating against high-molecular carbon increasing less complex carbon for GHG production [4, 24]. On the other hand, in terrestrial PF inundated for multiple centuries, microbial abundance decreased hinting that sea water can act as a stress factor for terrestrial microbial communities [25], which might lower CO_2 as well as CH_4 production.

During the Holocene, the Utqiaġvik peninsula (northernmost part of the Arctic Coastal Plain of Alsaka) underwent multiple marine regressions and transgressions, leading to the deposition of marine sediments now overlain by terrestrial layers [6, 26]. These paleoenvironmental processes shaped the current landscape, as reflected in the landscape positions of DLBs and ULs. DLBs, being topographically lower, are more likely to have PF influenced by marine deposits, while only deeper PF in ULs may contain marine sediments. The environmental conditions prevailing during sediment deposition shape microbial communities and influence their responses to thaw [27]. Additionally, marine sediment geochemistry, such as higher salinity and SO_4^{2-} pool, likely affects carbon production as well [4]. In a warming Arctic, sea water intrusion may affect differently PF carbon response depending on its marine influence, yet the role of microscale landscape and sediment history in GHG production during sea water inundations remains underexplored.

In our study, we investigated the carbon cycling response to sea water inundation considering different landscape histories. We simulated PF thaw under a salinity gradient for two cores corresponding to two main landscape features on the Utqiaġvik peninsula: an UL and a DLB core. To cover the vertical heterogeneity of the cores, we incubated four layers with distinct sedimentary composition under three water saltwater treatments and measured CO_2 and CH_4 production. We hypothesized that (1) the landscape history will result in different GHG production under sea water treatments, with higher CH_4 production from initially wetter site; (2) CH_4 will decrease with increase of salinity independently of the site history while CO_2 production will vary based on the landscape history.

2 | Material and Methods

To assess the research questions, an ex situ anaerobic incubation with two PF cores representing a former anoxic and oxic soil environment was conducted at 10°C for 368 days. To determine CO_2 and CH_4 production under different salt contents, three salt treatments were applied to incubation samples: a control treatment without salt added, a brackish water treatment, and a sea water treatment.

2.1 | Site Description and Sampling

The sampling site was located on the Utqiaġvik, formerly known as Barrow, Peninsula (the northernmost place of the United States; north of 71° latitude, Figure 1a), which is part of the Arctic Coastal Plain of Alaska. Historically, the Arctic Coastal Plain was shaped by multiple marine regressions during the late Cenozoic. The Utqiaġvik Peninsula belongs to the Younger Outer Coastal Plain that is characterized by Quaternary marine sediments covered by marine sands and silts [6, 18, 26]. The peninsula topography is flat, underlain by continuous PF and mostly covered by thaw lakes, DLBs, and interstitial polygonal tundra [18, 28, 29]. The mean annual temperature in Utqiaġvik, which lies about 12 km west of the sampling site, is −10.2°C with a maximum of 5.4°C in July and a minimum of −24.4°C in February (Alaska Climate Research Center [30], period from 1991 to 2020). The precipitation at the sampling site is dominated by snow with a mean annual precipitation of 136.9 mm (Alaska Climate Research Center [30], period from 1991 to 2020). The dominant vegetation depends on the landscape feature. The polygonal uplands are mainly composed of *Carex* and *Luzula*, while the DLB is dominated by *Carex*, *Eriophorum*, and *Sphagnum* mosses [29, 31].

Two PF soil cores were taken in April 2022 during the 2022 Alaska North Slope sampling campaign of the Alfred Wegener

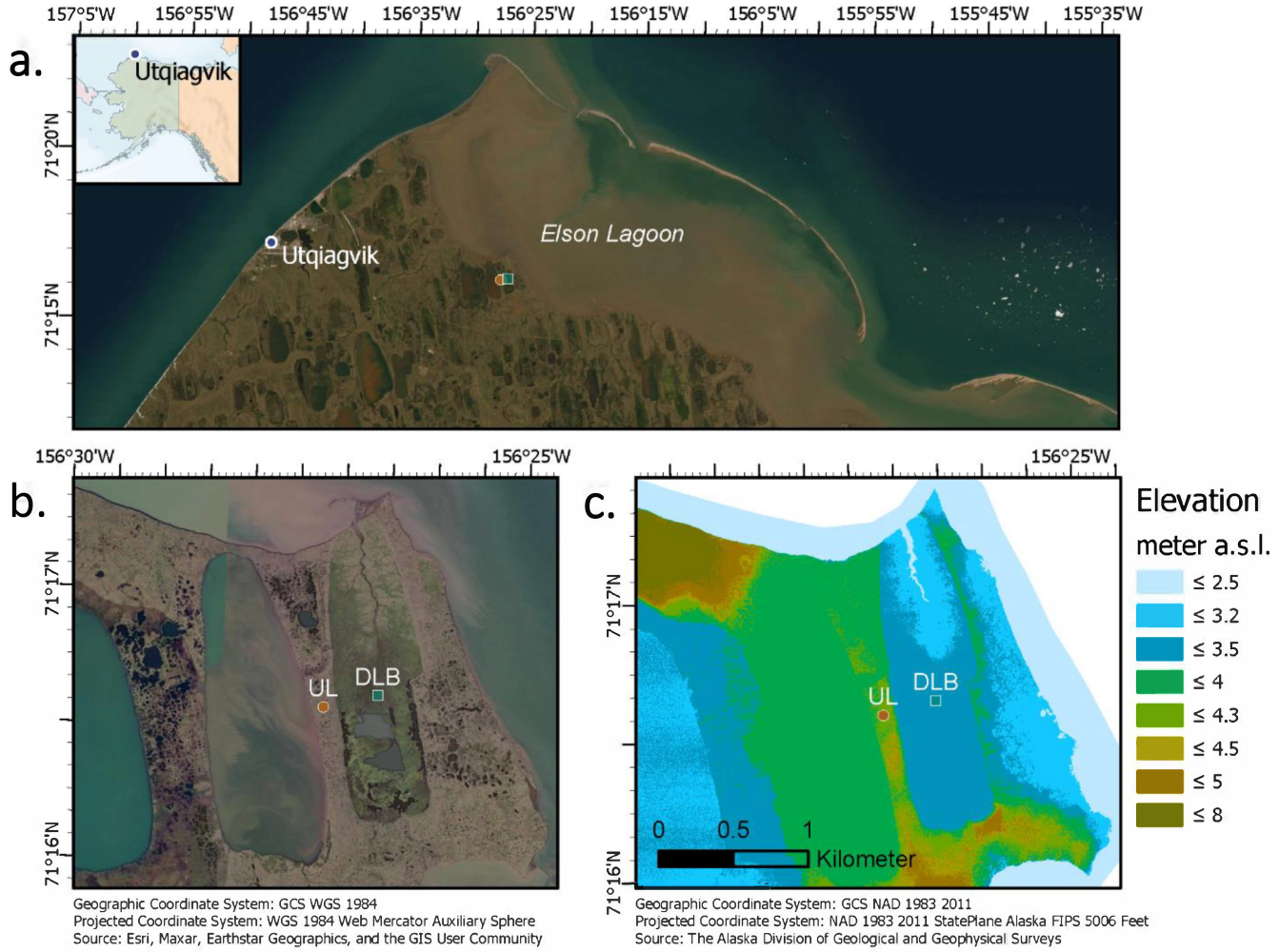

FIGURE 1 | Sampling sites of the two PF cores. Panels (a) and (b) show satellite images of the sampling area at different scales. Panel c shows the elevation above sea level (a.s.l.). DLB refers to the landscape position drained lake basin and UL refers to upland. The map was created with ArcGIS.

Institute (AWI) Potsdam. To represent the two most abundant landscape positions of the Arctic Coastal Plain, one 142-cm-long core was sampled at a DLB connected to the Elson Lagoon via a small stream (DLB core; N 71.27720°; W 156.44311°; elevation: 3 m a.s.l.). A second core of 204 cm was sampled about 300 m westward and about 1 m higher within interstitial tundra (UL core; N 71.27637°; W 156.45296°; elevation: 4 m a.s.l.) (Figure 1b,c). Additionally, the site locations were chosen due to their proximity to the coast and therefore potential seawater flooding in the near future [32]. Since the expedition happened in winter, it was not possible to measure the active layer thickness at both sites. Therefore, we used the values from Nyland et al. [33] monitored in Utqiagvik (N 71.31667°; W 156.5833°) between 2017 and 2021 to assess the active layer thickness for both sites (i.e., ranging from 34 to 43 cm).

For sampling, snow was removed from the sampling sites, then cores were drilled with a modified "Snow, Ice and PF-Establishment" (SIPRE) corer (Jon Holmgren's Machine Shop, Alaska, USA; diameter: 7.5 cm). A visual description of both cores can be found in the Supporting Information (Figure S1). Core segments were wrapped in plastic foil, labeled, and stored frozen during the transport to AWI Potsdam.

2.2 | Subsampling

Subsampling of the two cores took place in a cold lab at −4°C. Sampling depths were selected to capture the vertical heterogeneity of the cores and therefore different responses to PF thaw and the treatments. After splitting the upper meter of each core in half lengthwise, four layers were initially chosen based on the vertical PF distribution: the top of the active layer corresponding to the first 10 to 15 cm of the cores (AL1) (vegetation removed), the transition zone (bottom of the active layer: AL2), the middle of the PF layer (PF1), and the bottom of the PF (PF2) (Table 1). Due to differences in geological history, the soil horizons of the two cores (UL and DLB) were not identical across the depth profile. In the UL core, a thick peat layer extended from 0 to 33 cm, followed by a silty, organic-rich layer from 33 to 84 cm, interrupted by ice bands. The bottom 15 cm consisted of alternating gray silt and ice bands. In the DLB, the upper 22 cm also consisted of peat, followed by a sandy silt layer extending from 22 to 71 cm, then a thin silt layer, and finally a layer of peaty silt. From 91 to 107 cm, alternating light and dark gray layers were observed (Figure S1). To ensure that each individual layer represented a consistent soil horizon while also allowing for comparisons across cores at equivalent positions (surface layer [AL1], PF

TABLE 1 | Sampling depth and soil horizon description for each site.

Site	Layer	Sampling depth (cm)	Soil horizon
Upland	AL1	0–10	Light brown peat
	AL2	33–45	Medium gray silt, organic intrusion
	PF1	74–84	Medium gray silt, organic intrusion
	PF2	88–103	Gray silt, ice-rich
Drained lake basin	AL1	0–15	Peat
	AL2	22–45	Fine sandy silt
	PF1	69.5–79	Fine sandy silt
	PF2	95–107	Dark and light gray

table [AL2], and PF [PF1, PF2]), slightly different depth ranges were subsampled for the same positions (Table 1).

The subsampled layers were split into two parts, with the smaller part used for pore water and sediment analysis and the bigger part for the incubation. To ensure that the incubations were running properly (i.e., no contamination) we had four methodological replicates per layer and treatment.

2.3 | Pore Water and Sediment Analyses

Electrical conductivity, pH, and dissolved organic carbon (DOC) content were measured in pore water extracted with a Rhizon soil moisture samplers with a membrane filter length of 5 cm (pore-size 0.15 μm, Rhizosphere Research Products, Netherlands). Electrical conductivity and pH were measured right after water extraction. For that around 3.5 mL of pore water were filled into a small glass vessel. First, the electrical conductivity was measured with a conductivity pocket meter with a reference temperature of 25°C (Cond 340i, WTW, Germany). Next, the pH was measured with a potentiometer (Multilab 540, WTW, Germany).

Leftover pore water was acidified with a 30% HCl solution in a ratio of 1-μL:1-mL pore water to inhibit biological processes. Acidified samples were stored at 4°C until DOC measurement conducted by catalytic combustion at 630°C (TOC-VCPH, Shimadzu, Japan).

SO_4^{2-} and Cl^- anions were measured with ion chromatography (ICS 2100, Dionex/Thermo Fisher Scientific, Germany).

For sediment analysis, samples were freeze-dried (Sublimator 3-4-5, Zirbus Technology, Germany) and milled (Pulverisette 5, Fritsch, Germany) to a particle size smaller than 2 mm.

Total carbon (TC), total organic carbon (TOC), and total inorganic carbon contents were determined with a total organic carbon analyzer (soliTOC Cube, Elementar, Germany). Total nitrogen (TN) contents were measured with a nitrogen analyzer (rapid Max N exceed, Elementar, Germany).

Sedimentological data from the same cores and acquired with the same methodology from Seemann et al. [34] were added to our sedimentological data to have a higher vertical resolution and additional soil parameters (^{14}C ages and grain size distribution, Figure 2, Table S2). The radiocarbon dating was conducted by the AWI MICADAS laboratory [35] for nine samples (four from the UL and five from the DLB). Plant remains were selected for most of the samples. However, no plant remain was found for UL PF2; therefore, bulk sediment was used. The Calib 8.20 and the IntCal20 calibration curve were used to calibrate the data [36, 37].

Before analyzing the samples for grain size distribution, the organic matter was removed by adding hydrogen peroxide for 4 weeks. The grain size distribution was measured with a Malvern Mastersizer 3000 laser particle size analyzer (measuring range 0.01–1000 μm) and analyzed with GRADISTAT 8.0 [38].

2.4 | Incubation

The incubation was designed to mimic a sea water inundation at two typical landscape positions on the Arctic Coastal Plain. Thus, soil samples of two PF cores were incubated for 368 days under dark and anaerobic conditions at 10°C. To test the effect of sea water on CO_2 and CH_4 production, three salt treatments were applied in the incubation: a control treatment (sterilized tap water), a brackish water treatment and a sea water treatment. These treatments were applied across four depths for each core. Additionally, four blanks for each core were added: one corresponding to each treatment and an additional empty one. In total, the incubation comprised 104 samples (Figure S2). The duration of the incubation and the temperature were chosen to ensure that the carbon response to the sea water treatments—specifically methanogenesis—will be captured [11].

For the incubation set-up, an anoxic glovebox was used during sample preparation to ensure oxygen-free conditions. The samples were thawed overnight at 4°C. The thawed samples were homogenized in the glovebox by gently kneading them. Then, 6–10 g of wet sample material was weighed into sterilized 120-mL glass incubation bottles. Water was added in a ratio of 1:1 (volume water: weight wet sample) according to the treatment to form a slurry. Lastly, incubation bottles were closed with a rubber septum and crimped with an aluminium cap.

The salt water treatments, artificial brackish water and sea water, were manufactured using the protocol of Koch et al. [39]: For the sea water treatment, a total of 42.84 g salts and, for the brackish water treatment, a total of 15.45 g salts were added to 1 L of MilliQ water (exact chemical composition in Table S1). The salt content in the sea water treatment was 34.5–34.8 $mg \cdot L^{-1}$ which is slightly higher than the normal salt content of 28–32 $mg \cdot L^{-1}$ observed near the sampling location [40]. In the brackish water treatment, the salt content was 12.6 $mg \cdot L^{-1}$.

2.5 | Gas Measurements

To measure the CO_2 and CH_4 production in incubation bottles, 5-mL headspace gas was extracted and the CO_2 and CH_4

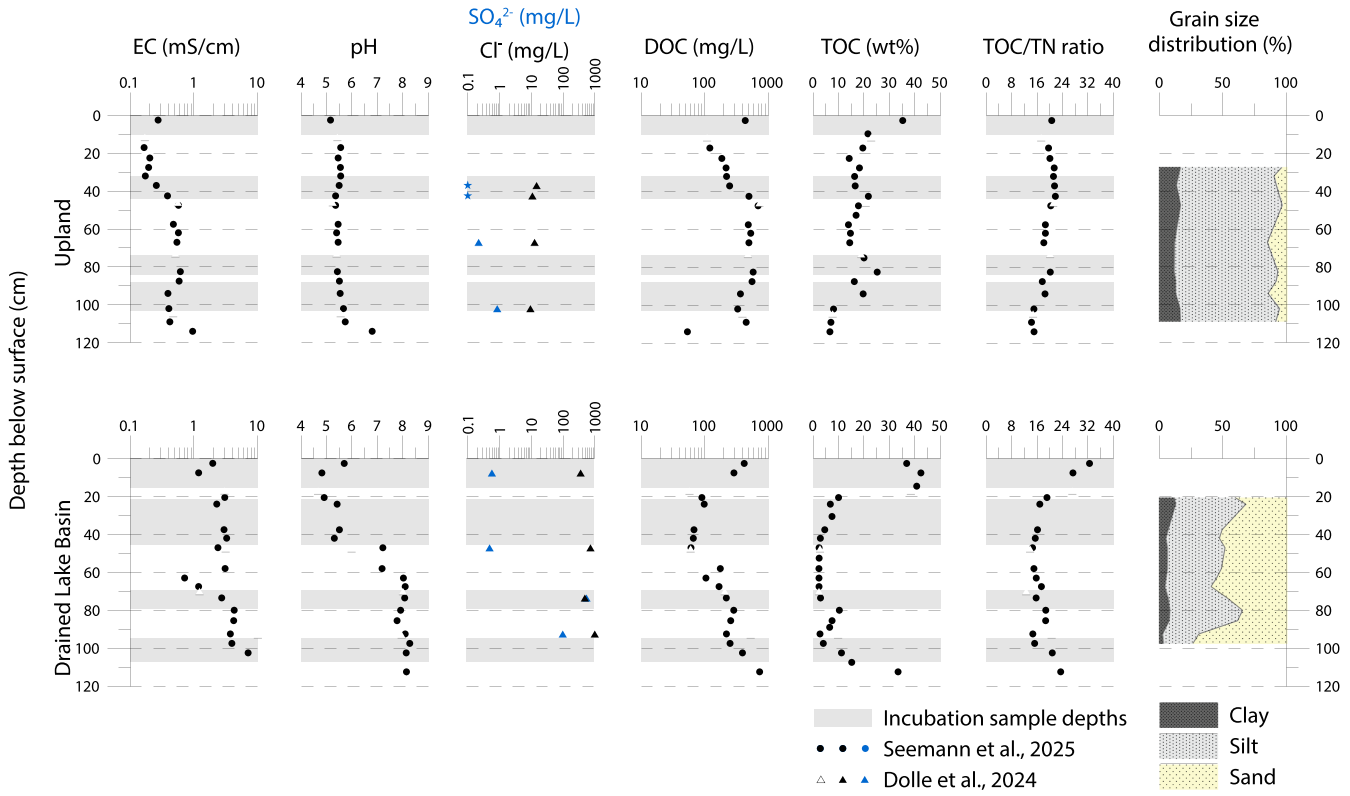

FIGURE 2 | Soil parameters of both cores. Electrical conductivity (EC), pH, chloride content (Cl^-), sulfate content (SO_4^{2-}), and dissolved organic carbon (DOC) were measured in pore water. Total organic carbon content (TOC), TOC/total nitrogen content (TN) ratio, ^{14}C ages, and grain sizes are sediment-based. Asterisks mark results below the detection limit of 0.1 mg/L. Please note that the SO_4^{2-} and Cl^- values at 75 cm for the DLB are similar and therefore overlap.

concentration was measured by a gas chromatograph (Nexis GC-2030, Shimadzu, Japan) with a flame ionization detector (FID) including a jetanizer (FID temperature: 400°C, makeup flow rate [N_2]: 26.2 mL/min, air flow rate: 200 mL/min). The minimum concentration measurable by the GC (detection limit) due to the calibration was 10 ppm.

Gas extraction was conducted using a 5-mL air tight glass syringe (SGE Analytical Science, Australia). In total, 5.5 mL of head space gas were extracted during sampling of which 0.5 mL were used for flushing the needle tip. To minimize the pressure disturbance due to the extraction of 5.5-mL gas from the sample, 5.5-mL N_2 was added after head space gas extraction.

To avoid excessive overpressure within the incubation bottles that could affect microbial activity, samples were flushed the following measurement day when they exceeded 10,000 ppm.

In the first week, CO_2 and CH_4 production was measured every 1–2 days and then every 7–10 days until day 100 and every 1 to 2 months after day 100.

2.6 | Data Processing and Analysis

Data processing, analysis, and plotting were conducted with R (4.3.1, R Core Team [41]) in RStudio (2023.06.1 + 524, Posit team [42]).

Raw GC data were transformed into daily production rates and cumulative productions in µg C per gram dryweight (g^{-1} DW) and also normalized per gram carbon (g^{-1} TOC) following the approach of Robertson et al. [43]. Thereby, gas concentrations in ppm were converted to µg CO_2-C or µg CH_4-C using the ideal gas law assuming a laboratory sampling temperature of 20°C. Additionally, gas concentrations were corrected for sampling dilution (5.5 mL), and the gas fraction dissolved in the water using Henry's Law. Gas production was then calculated as difference between gas concentrations of two consecutive measurements. The gas production was divided by the number of days between the measurements to obtain the production rates. The cumulative production was calculated from the sum of the gas production over the incubation time.

For quality control, two procedures were added to data processing. First, all CO_2 and CH_4 production rates below the mean change rate of procedural blank samples were excluded as not detectable. Second, a visual check for anomalies was conducted. Atypical samples were excluded if the anomaly was high in context with other replicates and measurements and if the GC chromatogram or a sampling note indicated a mistake. Finally, processed data [44] was saved for data analysis.

To assess differences between the landscape positions, only the control treatment was used. Two-way analysis of variances (ANOVAs) were conducted with cumulative CO_2 and CH_4 production at the end of the incubation. Since ANOVA requirements (normality, equal variances and independence) were not met in

some cases, data was logarithmic transformed before ANOVAs. As posthoc test, pairwise t-tests with Bonferroni adjustment were carried out. Additionally, CH_4 lag times were determined as defined from Treat et al. [15] as the time needed to reach the max. CH_4 production rate.

For comparison of treatment effects, a response factor per layer and treatment was calculated by normalizing the median production of a sample to the median production of the respective layer control treatment samples and subtracting one (which is the median production of the control treatment). Thus, a response factor of 0 represents the median cumulative production of the control treatment. A response factor smaller 0 means a lower production than the control treatment and a response factor higher 0 means a higher production than the control treatment. Significance in differences in CO_2 and CH_4 response between treatments (control treatment vs. brackish water and sea water treatment) was tested by paired t-tests.

3 | Results

3.1 | Pore Water and Sediment Parameters

The two landscape positions showed two distinct soil conditions across depths. The UL profile was relatively homogeneous across depth with respect to TOC, grain size distribution, pH, SO_4^{2-}, Cl^- and radiocarbon age (Figure 2, Table S2). Overall, the UL core had lower values for electrical conductivity, pH and SO_4^{2-} than DLB. In the DLB profile there was a differentiation between the pore water and the sediment characteristics between the deeper soil (>80 cm) and the upper layer in pH, electrical conductivity, Cl^-, SO_4^{2-} (Figure 2). ^{14}C ages were also significantly younger carbon in the layer up to 55 cm (676 ± 53 years BP to 2103 ± 239 years BP) than in deeper layers (~10,000 years BP; Table S2).

3.2 | Landscape Position Effect on CO_2 and CH_4 Production

3.2.1 | Cumulative Gas Production at the Incubation End

After 368 days, the general trend was that cumulative CO_2 and CH_4 production decreased with depth at both sites (Figure 3). On a dry weight basis (Figure 3a,b), gas production in the AL1 layer was four to five times higher at the DLB site (9270 CO_2-C g^{-1} DW and 10,900 CH_4-C g^{-1} DW) than at the UL site (2440 CO_2-C g^{-1} DW and 2010 CH_4-C g^{-1} DW). In all layers below, the production of CO_2 and CH_4 production decreased at both sites. CO_2 production ranged from 178 to 442 µg CO_2-C g^{-1} DW at the UL site and from 128 to 343 CO_2-C g^{-1} DW at the DLB site. CH_4 production ranged from 14.8 to 475 CH_4-C g^{-1} DW at the UL and from 80.3 to 439 CH_4-C g^{-1} DW at the DLB site. One layer created an exception to the depth trend on a dry weight basis: the PF1 layer at the DLB site where the lowest CO_2 (median: 128 µg C g^{-1} DW) and CH_4 production (median: 80.3 µg C g^{-1} DW) of that site was observed (Figure 3b).

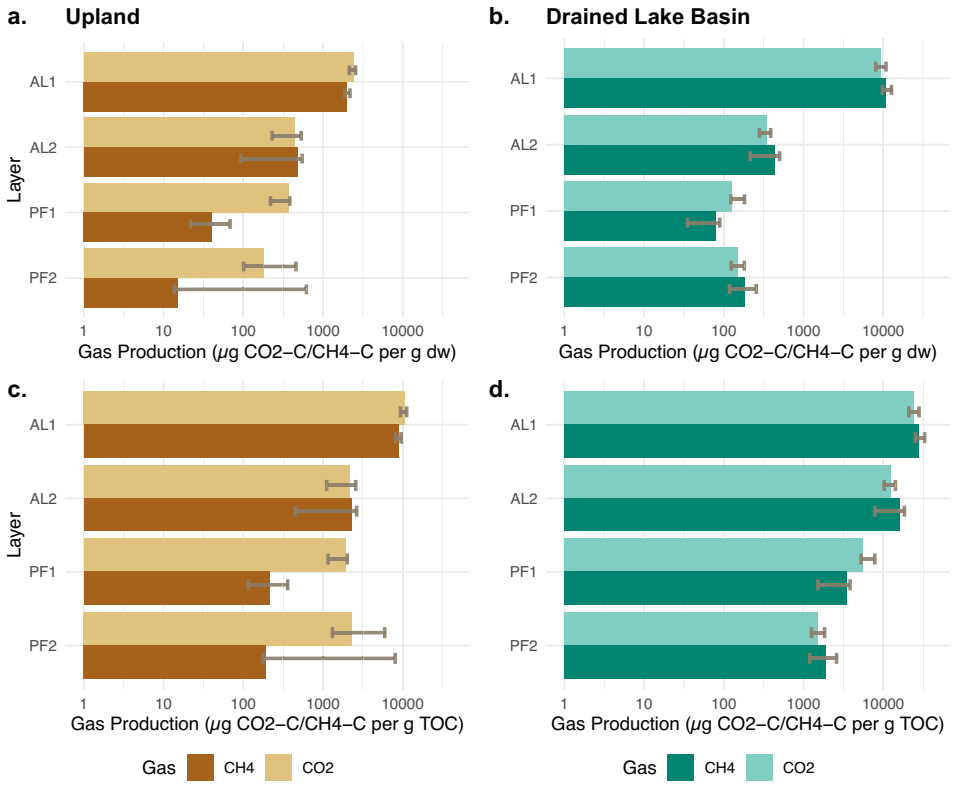

FIGURE 3 | Cumulative anoxic CO_2 and CH_4 production by layer at day 368 of the incubation in the control treatment (no salt added). Panels a and b show the gas production on a dry weight basis. Panels c and d show the gas production on a carbon basis. The bar represents the median of four replicates. Error bars show the range of the four replicates (min. to max.). Please note the logarithmic x-axis.

On a carbon basis, cumulative median CO_2 and CH_4 production were higher at the DLB site than the UL site (Figure 3c,d). The CO_2 production ranged from 1930 to 10,700 μg CO_2-C g^{-1} TOC at the UL site and from 1510 to 24,300 μg CO_2-C g^{-1} TOC at the DLB site (Figure 3c,d). One hundred ninety-three to 8780 μg CH_4-C g^{-1} TOC and 1890 to 28,300 μg CH_4-C g^{-1} TOC were produced at the UL and DLB site, respectively. At the UL site, the PF2 layer created an exception from the depth trend on a carbon basis. Here, CO_2 and CH_4 production were similar to the PF1 layer of that core (Figure 3c).

ANOVA results (Table 2) suggested that both site and layer were important controls in regulating CO_2 and CH_4 production. For CO_2 production, layer was the most important factor, but also the interaction between site and layer had a significant impact on CO_2 production. For CH_4 production, layer was again the most important factor. Site also played a significant role in CH_4 production, while there was no significant interaction between site and layer for CH_4 production.

Overall, gas production generally decreased with depth at both sites. At the DLB site, cumulative CO_2 and CH_4 production on a carbon basis were higher at the UL site. Layer and site were important factors for cumulative CO_2 and CH_4 production according to the ANOVA.

3.2.2 | CH_4 Production Dynamic Throughout the Incubation

When assessing gas production dynamics (Table 3), differences in CH_4 production between the two landscape positions became evident. At the DLB site, CH_4 production was stronger than at the UL site. This can be seen in the max. CH_4 production rates that were up to 10 times higher on a dry weight basis and up to 25 times higher on a carbon basis at the DLB site than at the UL site. Furthermore, the time to reach maximum CH_4 production rates, the CH_4 lag time, was shorter at the DLB site than at the UL site. In the AL1 layer, the DLB site had

TABLE 2 | Landscape position effect: ANOVA results for importance of the effects site and layer and the interaction effect of site and layer on cumulative CO_2 and CH_4 production on a DW and carbon basis at incubation end.

	CO_2				CH_4			
	DW		TOC		DW		TOC	
Effect	***p*-value**	**Sign.**	***p*-value**	**Sign.**	***p*-value**	**Sign.**	***p*-value**	**Sign.**
Site	8.72×10^{-1}		2.11×10^{-8}	***	2.00×10^{-3}	**	9.40×10^{-7}	***
Layer	2.02×10^{-17}	***	3.51×10^{-12}	***	9.43×10^{-11}	***	9.31×10^{-8}	***
Site:layer	8.98×10^{-7}	***	2.78×10^{-7}	***	1.61×10^{-1}		2.27×10^{-1}	

**p-value < 0.01, significant.
***p-value < 0.001, highly significant.

TABLE 3 | Max. CH_4 production rates, CH_4 lag time, min. CO_2:CH_4 rates with the control treatment at both sites.

	Depth	Max. CH_4 production rate		CH_4 lag time	Min. CO_2:CH_4	
	(cm)	(g dw)	(g TOC)	(days)	(ratio)	(day)
Upland	0–10 (AL1)	10.2 [8.49, 10.7]	44.4 [37.2, 46.7]	147 [68.0, 292]	1.21 [1.07, 1.27]	368 [368, 368]
	33–45 (AL2)	3.67 [0.563, 5.15]	17.7 [2.72, 24.9]	330 [292, 368]	0.958 [0.918, 2.47]	368 [368, 368]
	74–84 (PF1)	0.272 [0.106, 0.555]	1.43 [0.561, 2.93]	297 [191, 368]	7.05 [5.41, 17.5]	368 [368, 368]
	88–103 (PF2)	0.0878 [0.0693, 5.07]	1.14 [0.900, 65.9]	191 [104, 292]	9.37 [0.714, 12.7]	292 [292, 368]
Drained lake basin	0–15 (AL1)	79.0 [77.7, 115]	205 [202, 298]	90.0 [85.0, 126]	0.591 [0.466, 0.716]	103 [85.0, 194]
	22–45 (AL2)	4.56 [3.77, 5.30]	168 [139, 195]	30.5 [27.0, 34.0]	0.597 [0.572, 0.661]	124 [43.0, 194]
	69.5–79 (PF1)	1.17 [0.332, 1.85]	50.3 [14.3, 79.7]	292 [229, 368]	1.62 [1.31, 3.49]	292 [229, 368]
	95–107 (PF2)	2.03 [1.77, 2.16]	20.6 [18.0, 22.0]	209 [95.0, 292]	0.577 [0.507, 0.631]	209 [126, 292]

Note: The numbers represent the median values with the minimum and maximum values in parentheses for $N = 4$.

a CH_4 lag time (90 days) that was about half as long as the UL site (147 days). In the AL2 layer, the DLB core reached max. CH_4 production rate fastest (30 days) while it took 330 days in the UL core to reach its maximum. In PF layers, both sites showed similar CH_4 lag times.

Additionally to a higher and faster CH_4 production at the DLB site, this site also produced more CH_4 than CO_2. The higher CH_4 production can be seen in Figure 3b,d and was also reflected in min. CO_2:CH_4 ratios (Table 3). Min. CO_2:CH_4 ratios at the DLB site were about 0.6 with the PF1 layer as an exception. While at the UL site, CO_2:CH_4 ratios were about 1 in AL1 and AL2 layers and 7–9 in PF layers. Here again, the DLB site was faster in reaching min. CO_2:CH_4 ratios than the UL site. The DLB site reached min. CO_2:CH_4 ratios in 103–124 days in AL1 and AL2 layers and 209–292 days in PF layers, while the UL site needed until the end of the incubation to reach its min. CO_2:CH_4 ratios. This also indicated that min. CO_2:CH_4 ratios at the UL site might not have been reach after 368 days.

To sum up, the active layers had higher max. CH_4 production rates and shorter lag times than PF layers at both sites. However, the DLB site showed faster and greater CH_4 production at all depths compared to the UL site.

3.3 | Salt Water Effect on CO_2 and CH_4 Production

3.3.1 | Response Factor at the Incubation End

The response of CO_2 and CH_4 production to salt water at the incubation end compared to the median cumulative production of the control treatment is shown in Figure 4.

Based on the CO_2 response factor at the end of the incubation (Figure 4a,b), there were three response groups to differentiate the sea water effect: First is the three lower layers (AL2, PF1, and PF2) of the UL site where the CO_2 production increased in general with salt water treatments. This increase was significantly higher in the PF2 layer of the UL site where the sea water treatment produced 3.5 times more CO_2 ($p = 0.017$) than the control treatment. Second is AL1 layers at both sites and the AL2 layer of the DLB site where CO_2 production lowered up to 0.6 times with salt water addition. This decrease in CO_2 production compared to the control treatment was significant with the sea water treatment in all three layers (UL AL1 layer: $p = 0.021$, DLB AL1 layer: $p = 0.001$, DLB AL2 layer: $p = 0.007$). Third is the PF layers at the DLB site where there was no significant difference in CO_2 production between salt water treatment and the control treatment. Although no significant difference was measured between DLB PF1 under brackish treatment and the control, the response factor was positive and of the same order of magnitude as that of UL PF1 for the same treatment.

CH_4 production reacted differently than the CO_2 production under salt water treatments. In all layers of both sites, CH_4 production was inhibited with salt water treatments and CH_4 was more inhibited with the sea water treatment than with the brackish water treatment if CH_4 was produced at all (Figures 4c,d and S6).

3.3.2 | Gas Production With Salt Treatments Throughout the Incubation

The strongest response in CO_2 production can be seen in the PF2 layer of the UL core (Figure 5) with a response factor of 4.5 at around 200 days with the sea water treatment. That layer also showed the strongest response with the brackish water treatment with a response factor of about 2 after 50 days.

In general, all layers showed an initial peak in the CO_2 response factor with the brackish water treatment during the incubation. The time needed until this initial peak differed between the sites and layers. At the DLB site, the initial CO_2 response peak with brackish water appeared quickly after the incubation started, while it needed 30–50 days at the UL site for the response to show (Figure 5). In the UL PF layers, the brackish water peak was followed by a CO_2 response peak with the sea water treatment.

The CH_4 production with salt treatments in PF layers at both sites was low to non-detectable (Figure 6). In active layers, CH_4 production decreased with both salt treatments at the start of the incubation. After that initial decrease in CH_4 production, the response became attenuated in the brackish water treatment towards the end of the incubation while with the sea water treatment CH_4 inhibition lasted throughout the whole incubation.

4 | Discussion

4.1 | Soil Characteristics

At the DLB site, pH, electrical conductivity, SO_4^{2-} and Cl^- content (Figure 2) indicate that the deeper layers (PF layers) likely had contact with sea water before the incubation, as pH and electrical conductivity of DLB PF layers are similar to brackish core sections of Siberian thermokarst lagoon sediments (pH: 7.5–8 and electrical conductivity: 3.3 mS/cm [8]). The sea water contact could have been caused by re-mobilized saline deposits [45] or by inundation. In this study, the gap of 8000 years in the radiocarbon dating (Table S2), as well as the inverse age at 110 cm compared to 79 cm, could indicate potential cryoturbation events, supporting re-mobilized saline deposits more than sea water intrusion. Indeed, lake drainage processes often result in deep thawing, surface subsidence, and refreezing, which can mix soils from different depositional episodes [19, 46]. However, in the absence of geomorphological evidence (e.g., involutions, frost cracks, or patterned ground), cryoturbation alone cannot account for such a substantial age gap. A more plausible explanation may involve erosion or truncation of the soil during thaw events, in combination with cryoturbation.

The UL site exhibits a clearly different soil environment compared to the DLB site concerning the pore water and sediment parameters (Figure 2). The parameters confirm the UL site as a primary surface, meaning that the landscape was not affected by thaw lake formation [47]. TOC at the UL site decreases with depth (about 35%–10%), supporting soil formation without disturbances [48]. Finally, the pH values are indicative of moist acidic tundras [17, 49].

To sum up, the soil characteristics at the UL and the DLB (Figure 2) reveal distinct patterns that depend on landscape

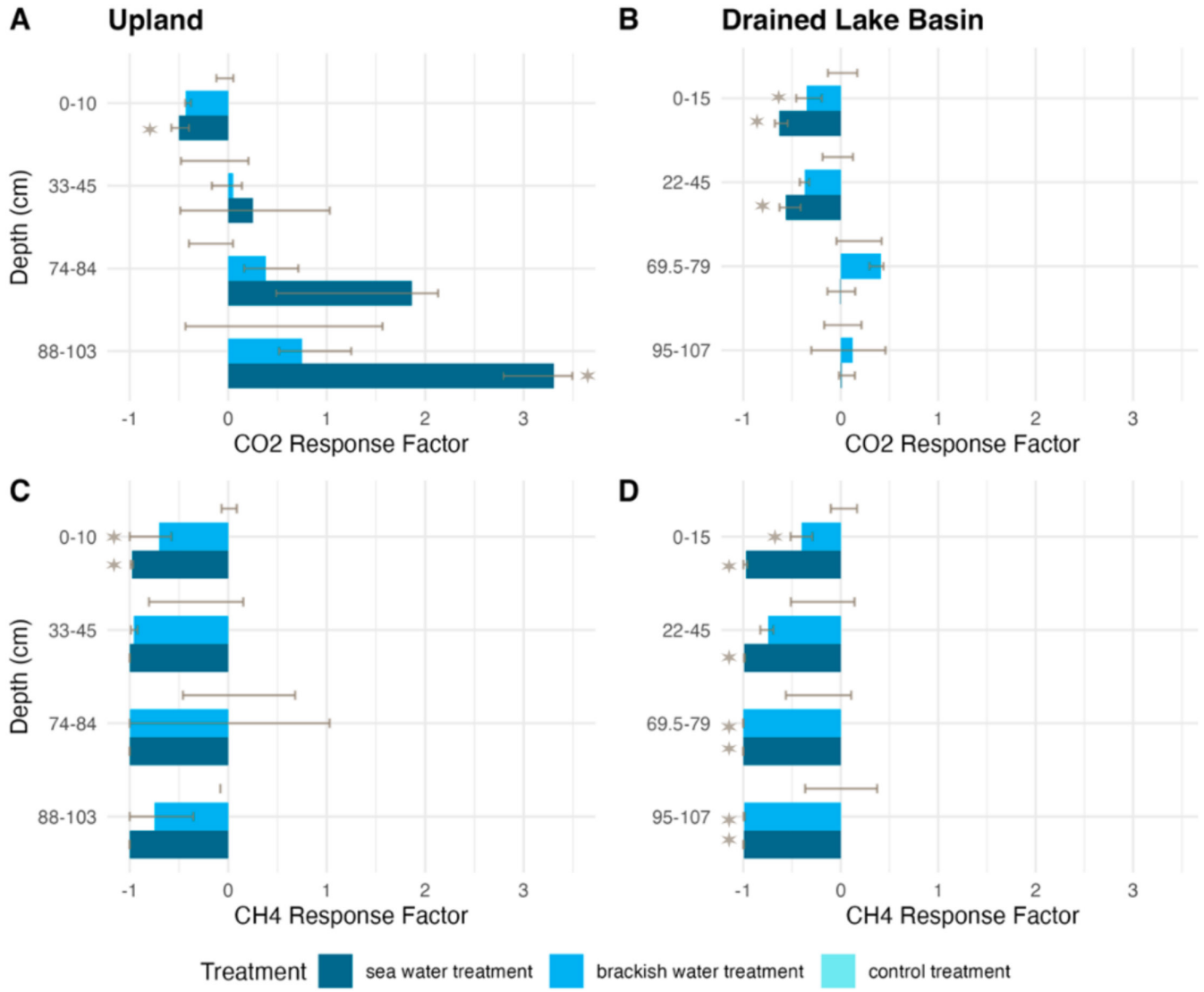

FIGURE 4 | CO_2 and CH_4 response to sea water treatments relative to the production under the control treatment. Panels (a) and (b) show the CO_2 response. Panels (c) and (d) show the CH_4 response. Bars represent the median over four replicates. Error bars indicate min to max of four replicates. For non-detectable CH_4 productions (DLB PF1 and UL PF layers with sw treatment), a production of 0 was assumed to calculate the response factor. Asterisks mark significant differences in the response factors to the control treatment.

history and position. While the UL appears to have experienced relatively constant soil formation, the talik formation prior to drainage in the genesis of the DLB may have altered carbon quality and re-mobilized deeper marine sediments [19]. The active layer of the DLB compares well to other DLBs on the Alaskan North Slope. The PF layers have been inundated by marine waters before this study as characteristic of the Utqiaġvik Peninsula [6, 26]. At the UL site, soil characteristics are similar to other primary surfaces in the region, with PF layers unaffected by earlier thawing.

4.2 | Landscape Position Effect

4.2.1 | Carbon Availability

A decrease in anaerobic CO_2 and CH_4 production with depth in PF soils is often linked to a decrease in carbon availability and quality [15, 50]. In this study, high TOC content in the AL1 layers (UL 35%, DLB 40%) coincides with the highest CO_2 and CH_4 production. Additionally, the DLB site with a 5% higher TOC content has a 4-time higher gas production than the UL site in that layer. In AL2, PF1 and PF2 layers, TOC is higher in the UL core which is concurrent with higher CO_2 productions than in the DLB core on a dry weight basis (Figures 2 and 3a,b). This is in accordance with previous studies showing the importance of soil carbon quantity for CO_2 production [15, 51, 52].

On a carbon basis, PF layers at the UL site produce very similar amounts of CO_2 and CH_4 after 368 days (Figure 3c). The CO_2 production is even similarly high as in the AL2 layer. As this site has been unaffected by former PF thaw, an initial burst of labile carbon may have become available upon PF thaw [53, 54]. Labile carbon may then have acted as a driver of CO_2 production in PF layers of the UL site. This effect is supported by the initially higher CO_2 production of the PF layers compared to the

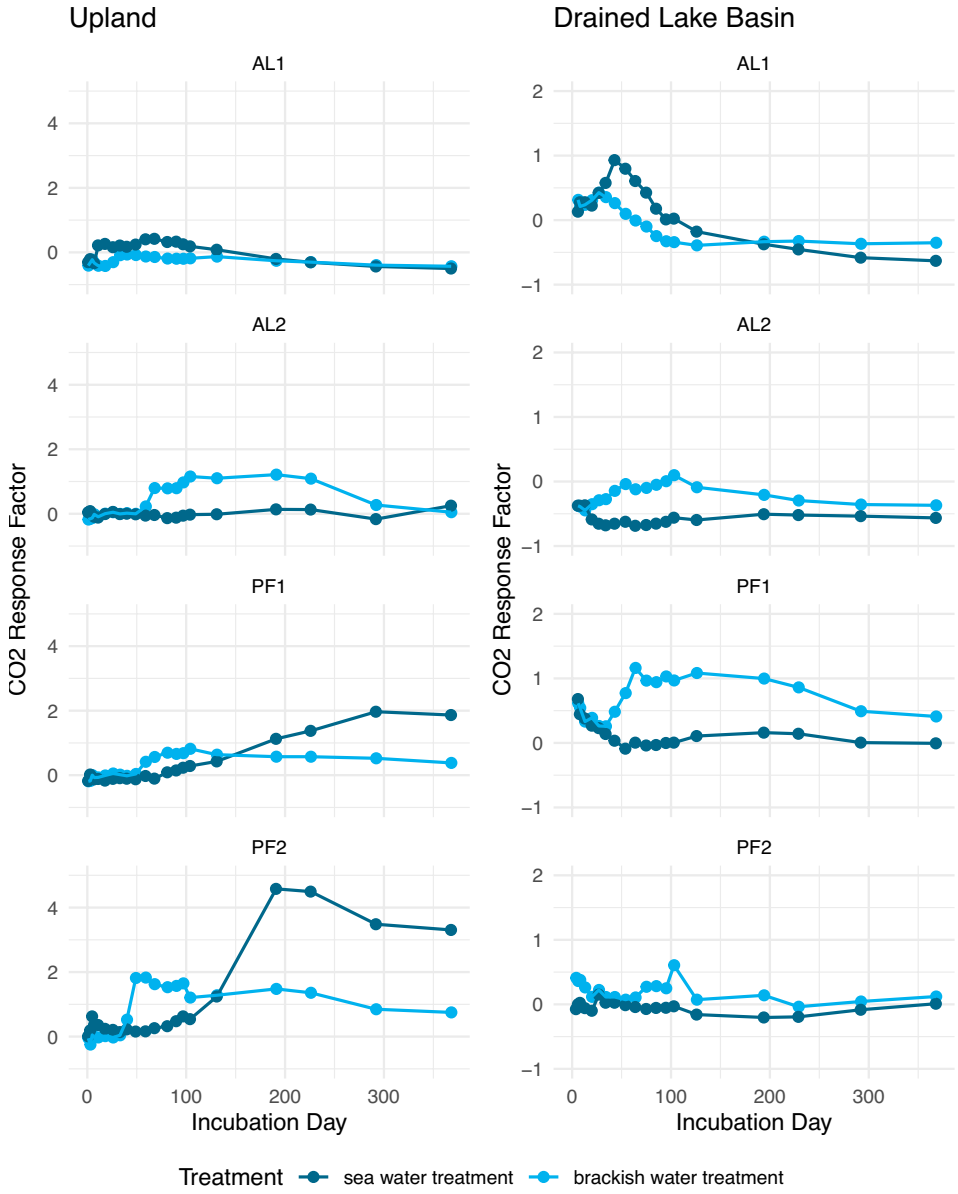

FIGURE 5 | Median CO_2 response factors to salt treatments throughout the incubation at both sites. Please note the different y-axis.

AL2 layer (Figure S4). After thaw, the PF layers of the DLB core exhibited a burst of CO_2 production as well. However, when normalized to carbon content, this production was two to five times lower than that observed in AL2 from the same core (Figure S3). As previously mentioned, the PF layers in the DLB core were likely affected by cryoturbation or erosion, indicating past thaw events. This prior thaw exposure may have reduced the lability of the carbon [55, 56], potentially explaining the lower CO_2 production compared to the UL layer. The results shown in this study are in accordance with the already established relations between CO_2 production and organic carbon quantity and quality.

4.2.2 | Microbial Adaptation

Prevailing anoxic soil conditions drive CH_4 production in PF soils [12, 57]. As the DLB lies relatively lower than the UL site, water-logged anoxic conditions will be more apparent especially in the active layers at the DLB site [14]. Thus, the microbial communities at the DLB site could be more adapted to anoxic conditions that were mimicked in the incubation than the microbial community at the UL site. This study support the idea of anoxic conditions driving CH_4 production with the higher CH_4 and CO_2 production on a carbon basis at the DLB than the UL site. Additionally, the high max. CH_4 production rates and low CO_2:CH_4 ratios (Figure 3, Table 3) also highlight the influence of already adapted microbial community to anoxic conditions.

With the DLB site being more adapted to anoxic soil conditions, the reduced CH_4 production on a dry weight basis in the PF1 layer at the DLB site (Figure 3b) is unexpected. Here, the former sea water contact of the PF layers might be an important control. Indeed, the electrical conductivity in the PF layers of DLB indicates brackish conditions in these layers. The

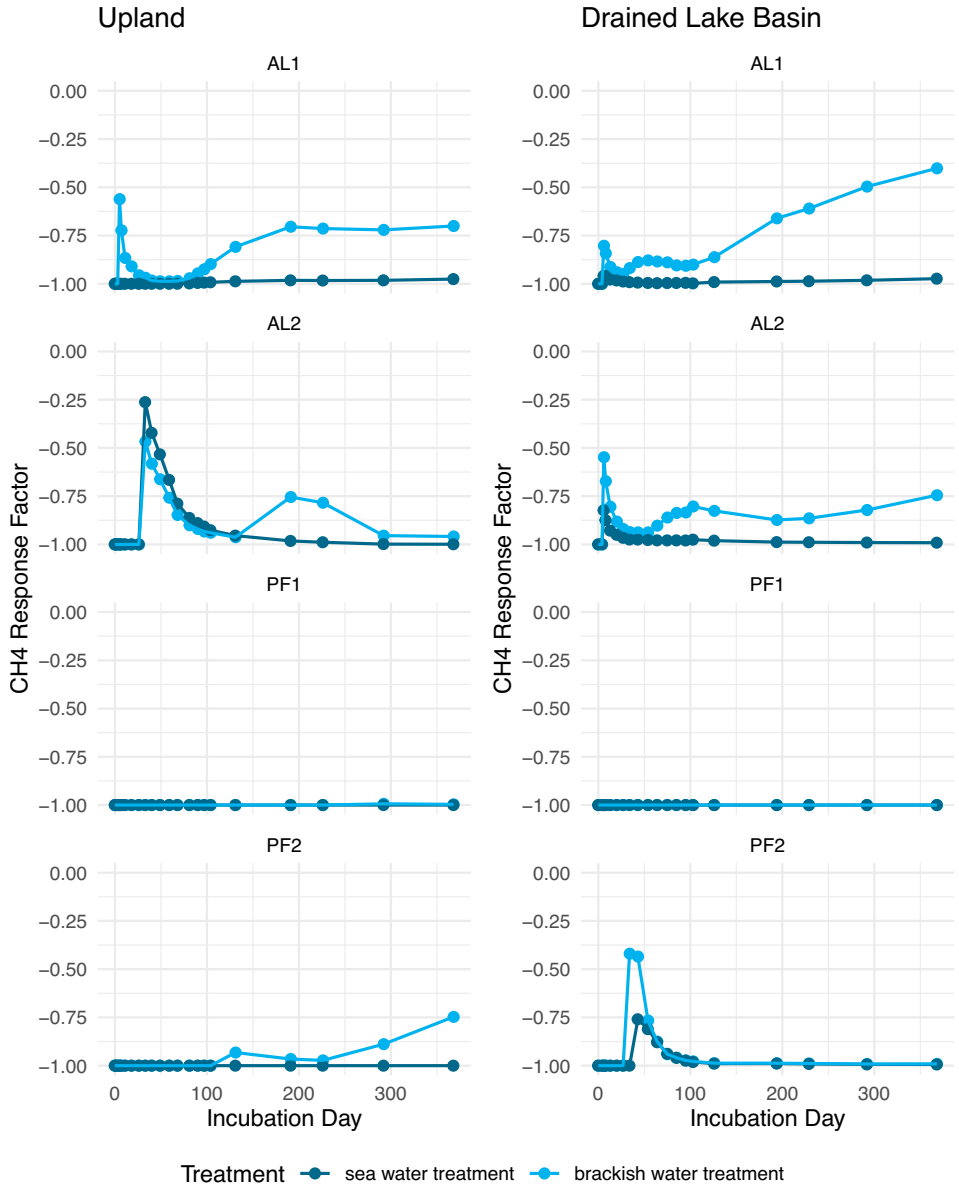

FIGURE 6 | Median CH_4 response factors to salt treatments throughout the incubation at both sites.

high SO_4^{2-} content in the PF1 layer at the DLB site (999 mg/L; Figure 2) can explain the low CH_4 production as SO_4^{2-} reduction is energetically more favorable than methanogenesis [58]. This is consistent with Yang et al. [23], where they found that CH_4 production decreases with salinity, but was not fully inhibited for low-lying flooded area under brackish conditions. The increase of SO_4^{2-} in the soil leads to an increase of SO_4^{2-}-reducing bacteria (SBR) which can be competitors for methanogenesis [23, 59]. To limit this competition, methanogens use mainly CO_2 or methanol metabolism pathways instead of organic compounds such as acetate [23, 60].

Overall, CO_2 and CH_4 production with the control treatment can be interpreted as an interaction of microbial adaptation to anoxic soil conditions, carbon availability and sea water exposure which combined form the landscape position effect.

4.3 | Salt Water Effect

4.3.1 | Carbon Availability

CO_2 production increased with sea water addition at both sites in certain layers (Figure 4). The same effect was observed in thawing coastal PF samples from thermokarst lake and thermokarst lagoon sediments on the Bykovsky Peninsula, Siberia, Russia, under anaerobic conditions [11] and from the Yukon Coast, Canada under aerobic conditions [4, 61]. As this effect has been observed under aerobic and anaerobic conditions, prevailing oxygen availability does not seem to be decisive for CO_2 production with salt water. Instead, a higher carbon availability due to the sea water addition is discussed as a possible reason for higher CO_2 production with sea water [4, 51, 61]. Sea water can cause complex carbon compounds to flocculate increasing the

mobility of less complex carbon [24] that could then be available for CO_2 production [4, 51, 61].

Conversely, the lack of response to sea water addition at the DLB site likely reflects its history of prior marine inundation and associated long-term changes in soil chemistry (Figure 2). These pre-incubation conditions may have already changed the carbon availability, minimizing the effect of additional salt inputs. This is supported by significantly higher CO_2-C per g TOC under control conditions at DLB compared to UL (Figure 3c,d), indicating that carbon was initially more available at DLB. In contrast, the UL site, which was not exposed to marine inundation, showed a stronger response, suggesting that sea water addition could have had a more pronounced effect on carbon mobilization and therefore explain the CO_2 response in AL2, PF1 and PF2 layers at the UL site (Figure 4).

The overall decrease in CO_2 production observed in UL AL1 (Figure 4) may be explained by the presence of a peat layer (Figures 2 and S1). In organic-rich soils (TOC > 20%), carbon is typically more available, often resulting in higher CO_2 production rates [15]. Therefore, in such peat layers, carbon availability might not be the limiting factor, and redox conditions could play a more dominant role in controlling CO_2 production.

4.3.2 | Electron Acceptors and Microbial Adaptation

In non-PF coastal environments, an inhibition of CH_4 production with sea water is observed as well [59, 62]. This CH_4 response is likely linked to the role of electron acceptors in sea water [58, 59, 62]. As SO_4^{2-} reduction is energetically more favorable than methanogenesis, the addition of SO_4^{2-} with the salt water treatments can hinder CH_4 production. In layers where CH_4 production was least inhibited by the brackish water treatment at the end of the incubation (meaning UL AL1 layer and DLB AL1 and AL2 layers), the initial SO_4^{2-} concentrations were the lowest (Figure 2). This could result in a smaller SO_4^{2-} pool for these layers and therefore, explain CH_4 production at the end of the incubation period. The CH_4 lag time could thus represent the time needed to deplete SO_4^{2-} as energy source.

This SO_4^{2-} reduction could also explain the initial peak in CO_2 production that happened in AL1 layers with sea and brackish water treatment (Figures 5 and S5). Now, when assuming a depletion of SO_4^{2-} as electron acceptor with the brackish water treatment within incubation duration it is possible to explain the stronger response in CO_2 (positively) and CH_4 (negatively) in AL1 layers with the higher amount of SO_4^{2-}.

At the DLB site, the PF most likely had contact with sea water before (Figure 2) making it reasonable to assume that microbes are adapted to brackish water conditions. The addition of sea water did not seem to change any relevant factors for CO_2 production leading to almost no differences between all three treatments. That CH_4 was produced with the control treatment and that at least twice as much CH_4 was produced in DLB compared to UL PF layers (Figure 3) indicates that active methanogens were present in the brackish water affected PF layers even though CH_4 production was inhibited when SO_4^{2-} was present. Other studies observed a similar behavior from low saline former PF environments, where CH_4 production declines significantly after sea water addition [11, 23].

Not only the availability of SO_4^{2-} is changed with the addition of salt water, but also the availability of other nutrients and pore water pH can be impacted by the treatments applied in this study. For example, the biogeochemical cycle of Cl^- on the Arctic Coastal Plain is linked to iron and humic substance cycling [63]. It is even discussed if organohalide respiration could inhibit CH_4 production similar to Fe (III) reduction (by reducing H_2 levels) [63]. Additionally, pH drives microbial communities in PF [50, 64] with methanogens being most productive at ranging between 6.5 and 7 [65, 66].

Furthermore, it is essential to consider the impact of rewetting and thawing on the CO_2 production. In the majority of the treatments, a peak in CO_2 production was observed at the beginning of the incubation. Many studies have shown that CO_2 exhibit a positive response following rewetting events [67–69]. The addition of water can facilitate the breakdown of the soil aggregates and make the organic matter more available for microbial communities [68, 70, 71]. These complex biogeochemical couplings make it impossible to pinpoint the exact cause for CO_2 and CH_4 response to sea water within the scope of this study.

In summary, the salt water effect on CO_2 and CH_4 production under anaerobic conditions can not solely be explained by a change in carbon availability. A key role is also played by the change in soil redox conditions due to salt addition, which shifts the availability of electron acceptors. Additionally, further biogeochemical aspects such as pH, nutrient availability or soil aggregate could affect the CO_2 and CH_4 response to salt water.

4.4 | Challenges in Comparing CO_2 and CH_4 Production Across Studies: Limitation, Implications, and Future Research

Directly comparing CO_2 and CH_4 production with other research is challenging due to the limited number of comparable incubation studies and the varying framework parameters used in these investigations (e.g., temperature, units, incubation duration [13, 15]). Cumulative CO_2 and CH_4 production with the control treatment in mineral (TOC below 30%) and organic (TOC higher 30%) layers are within the same range as the anaerobic gas production observed at 15°C from moist acidic Alaskan PF soils incubated for 500 days [13]. Compared to anoxic PF incubations on a pan-arctic scale, median CO_2 production rates are at least two times lower in this incubation at the respective landscape positions ([15]: 52.1 $\mu g\ g^{-1}\ C^{d-1}$ [UL]; 125 $\mu g\ g^{-1}\ C^{d-1}$ [DLB]). Median CH_4 production rates on the other hand are at least 4 times higher than max. production rates at the DLB ([15]: 0.6 $\mu g\ g^{-1}\ C^{d-1}$ [DLB]) while they seem to be lower at the UL site ([15]: 8.2 $\mu g\ g^{-1}\ C^{d-1}$ [UL]). The anaerobic CO_2 production with sea water (Figure S5) is generally lower than CO_2 production with sea water at 4°C under aerobic conditions [61].

This study investigated the production of CO_2 and CH_4 under anaerobic conditions mimicking PF thaw accompanied by sea water inundation. However, the actual amount of carbon GHG released to the atmosphere is also impacted by factors

not covered in this study. For example, the transport process of GHG from soil to the atmosphere by exudation through plants or by ebullition can have a significant impact on the GHG flux [16, 72, 73]. During transport CH_4 can be oxidized to CO_2 within the sediment and water column in thaw lakes [74, 75] as well as in marine environments [23, 76]. Additionally, soil temperature sensitivity [51, 74, 77, 78], effects of freeze–thaw events [49, 79], influences of water-level changes [16], and effects of sea water composition [24] are aspects not within the scope of this study. Nevertheless, CO_2 and CH_4 production form the basis of GHG fluxes and ex-situ incubations have shown to effectively reproduce in situ anaerobic carbon cycling dynamics, such as CO_2 and CH_4 productions [80, 81]. Finally, it is important to note that this study is based on only two soil cores. Although these were selected to represent the two most common landscape features in the area, they do not encompass the full heterogeneity of the PF landscape. Therefore, based on the results from this case study, we recommend further investigations into the effects of sea water inundation across a wider range of PF landforms, including sites with diverse landscape histories.

5 | Conclusions

The results of this case study show that site history can largly impact CO_2 and CH_4 production. Without sea water, the initially wetter site (DLB) exhibits a higher CH_4 production which is caused by an interplay of site history, microbial adaptation and carbon availability. Furthermore, with the addition of sea water, results show that sea water inundation of terrestrial PF has differencing effects on CO_2 and CH_4 production. The CH_4 production decreases with the increase of salt concentration even when the microbial community was already adapted to brackish conditions, that is, equal production of CO_2 and CH_4. The addition of SO_4^{2-} is likely to explain this behavior, as SO_4^{2-} reduction is energetically more favorable than methanogenesis. Thus, our findings support the hypothesis that redox conditions seem to be a stronger controlling factor than microbial adaptation for CH_4 production. The response of CO_2 is more variable and appears to be contingent on the site history. In particular, no response to the salt addition was observed for the layers that have been exposed to sea water intrusion before this incubation. However, for non-marine-affected soils, the salt addition may intensify the carbon availability as well as nutrient availability and lead to a positive feedback in CO_2 production. Here we highlight the effect of salt on CH_4 and CO_2 production in a controlled ex-situ experiment where soil dynamics are not considered. In future studies, it is therefore necessary to examine the effect of sea level rise on GHG production under conditions closer to reality, where vertical and lateral soil dynamics are taken into account.

Acknowledgments

Funding for this study was provided by European Research Council Starting Grant 851181 (FluxWIN). The authors would like to thank Guido Grosse and Benjamin Jones for leading the Arctic field campaign in April 2022 and for their participation in the coring; Kenneth M. Hinkel is gratefully thanked for providing the drilling equipment (SIPRE corer). We also thank the Ukpeaġvik Iñupiat Corporation (UIC) for excellent logistical support; Justin Lindemann, Antje Eulenburg, Daniel Warner, and all AWI Potsdam lab technicians for their help with lab work; Lars Johann Ebel for the soil parameter figure; and the reviewers for their helpful comments. Open Access funding enabled and organized by Projekt DEAL.

Conflicts of Interest

The authors declare no conflicts of interest.

Data Availability Statement

The data sets used in this paper are available at https://doi.org/10.1594/PANGAEA.969147 and https://doi.org/10.1594/PANGAEA.969148.

References

1. H. Lantuit, P. P. Overduin, N. Couture, et al., "The Arctic Coastal Dynamics Database: A New Classification Scheme and Statistics on Arctic Permafrost Coastlines," *Estuaries and Coasts* 35 (2012): 383–400, https://doi.org/10.1007/s12237-010-9362-6.

2. M. Fritz, J. E. Vonk, and H. Lantuit, "Collapsing Arctic Coastlines," *Nature Climate Change* 7 (2017): 6–7, https://doi.org/10.1038/nclimate3188.

3. A. M. Irrgang, M. Bendixen, L. M. Farquharson, et al., "Drivers, Dynamics and Impacts of Changing Arctic Coasts," *Nature Reviews Earth and Environment* 3 (2022): 39–54, https://doi.org/10.1038/s43017-021-00232-1.

4. G. Tanski, D. Wagner, C. Knoblauch, M. Fritz, T. Sachs, and H. Lantuit, "Rapid CO_2 Release From Eroding Permafrost in Seawater," *Geophysical Research Letters* 46 (2019): 11244–11252, https://doi.org/10.1029/2019GL084303.

5. A. E. Gibbs and B. M. Richmond, "National Assessment of Shoreline Change—Summary Statistics for Updated Vector Shorelines and Associated Shoreline Change Data for the North Coast of Alaska, US-Canadian Border to Icy Cape, Report US Geological Survey Reston, VA," 2017, https://pubs.usgs.gov/of/2017/1107/.

6. M. T. Jorgenson and J. Brown, "Classification of the Alaskan Beaufort Sea Coast and Estimation of Carbon and Sediment Inputs From Coastal Erosion," *Geo-Marine Letters* 25 (2005): 69–80, https://doi.org/10.1007/s00367-004-0188-8.

7. M. Angelopoulos, P. P. Overduin, S. Westermann, et al., "Thermokarst Lake to Lagoon Transitions in Eastern Siberia: Do Submerged Taliks Refreeze?," *Journal of Geophysical Research: Earth Surface* 125 (2020): e2019JF005424, https://doi.org/10.1029/2019JF005424.

8. M. Jenrich, M. Angelopoulos, G. Grosse, et al., "Thermokarst Lagoons: A Core-Based Assessment of Depositional Characteristics and an Estimate of Carbon Pools on the Bykovsky Peninsula," *Frontiers in Earth Science* 9 (2021): 637899, https://doi.org/10.3389/feart.2021.637899.

9. J. Strauss, M. Fuchs, G. Hugelius, et al., "Organic Matter Storage and Vulnerability in the Permafrost Domain," in *Encyclopedia of Quaternary Science*, 3rd ed. (Elsevier, 2025), https://doi.org/10.1016/B978-0-323-99931-1.00164-1.

10. E. A. Schuur, B. W. Abbott, R. Commane, et al., "Permafrost and Climate Change: Carbon Cycle Feedbacks From the Warming Arctic," *Annual Review of Environment and Resources* 47 (2022): 343–371, https://doi.org/10.1146/annurev-environ-012220-011847.

11. M. Jenrich, M. Angelopoulos, S. Liebner, et al., "Greenhouse Gas Production and Microbial Response During the Transition From Terrestrial Permafrost to a Marine Environment," *Permafrost and Periglacial Processes* 36 (2025): 63–82.

12. M. Laurent, M. Fuchs, T. Herbst, A. Runge, S. Liebner, and C. C. Treat, "Relationships Between Greenhouse Gas Production and Landscape Position During Short-Term Permafrost Thaw Under Anaerobic

Conditions in the Lena Delta," *Biogeosciences* 20 (2023): 2049–2064, https://doi.org/10.5194/bg-20-2049-2023.

13. H. Lee, E. A. G. Schuur, K. S. Inglett, M. Lavoie, and J. P. Chanton, "The Rate of Permafrost Carbon Release Under Aerobic and Anaerobic Conditions and Its Potential Effects on Climate," *Global Change Biology* 18 (2012): 515–527, https://doi.org/10.1111/j.1365-2486.2011.02519.x.

14. C. S. Sturtevant and W. C. Oechel, "Spatial Variation in Landscape-Level CO_2 and CH_4 Fluxes From Arctic Coastal," *Global Change Biology* 19 (2013): 2853–2866, https://doi.org/10.1111/gcb.12247.

15. C. C. Treat, J. Ernakovich, C. M. Iversen, et al., "A Pan-Arctic Synthesis of CH_4 and CO_2 Production From Anoxic Soil Incubations," *Global Change Biology* 21 (2015): 2787–2803, https://doi.org/10.1111/gcb.12875.

16. T. Eckhardt, C. Knoblauch, L. Kutzbach, et al., "Partitioning Net Ecosystem Exchange of CO_2 on the Pedon Scale in the Lena River Delta, Siberia," *Biogeosciences* 16 (2019): 1543–1562, https://doi.org/10.5194/bg-16-1543-2019.

17. N. Taş, E. Prestat, S. Wang, et al., "Landscape Topography Structures the Soil Microbiome in Arctic Polygonal Tundra," *Nature Communications* 9 (2018): 777, https://doi.org/10.1038/s41467-018-03089-z.

18. K. M. Hinkel, W. R. Eisner, J. G. Bockheim, F. E. Nelson, K. M. Peterson, and X. Dai, "Spatial Extent, Age, and Carbon Stocks in Drained Thaw Lake Basins on the Barrow Peninsula, Alaska," *Arctic, Antarctic, and Alpine Research* 35 (2003): 291–300, https://doi.org/10.1657/1523-0430(2003)035[0291:SEAACS]2.0.CO;2.

19. B. M. Jones, G. Grosse, L. M. Farquharson, et al., "Lake and Drained Lake Basin Systems in Lowland Permafrost Regions," *Nature Reviews Earth and Environment* 3 (2022): 85–98, https://doi.org/10.1038/s43017-021-00238-9.

20. K. R. Reddy and R. D. DeLaune, *Biogeochemistry of Wetlands: Science and Applications* (CRC Press, 2008).

21. C. G. Andresen, D. M. Lawrence, C. J. Wilson, et al., "Soil Moisture and Hydrology Projections of the Permafrost Region—A Model Intercomparison," *Cryosphere* 14 (2020): 445–459.

22. S. Shahariar, R. Farrell, R. Soolanayakanahally, and A. Bedard-Haughn, "Elevated Salinity and Water Table Drawdown Significantly Affect Greenhouse Gas Emissions in Soils From Contrasting Land-Use Practices in the Prairie Pothole Region," *Biogeochemistry* 155 (2021): 127–146.

23. S. Yang, S. E. Anthony, M. Jenrich, et al., "Microbial Methane Cycling in Sediments of Arctic Thermokarst Lagoons," *Global Change Biology* 29 (2023): 2714–2731, https://doi.org/10.1111/gcb.16649.

24. F. Dou, C. Ping, L. Guo, and T. Jorgenson, "Estimating the Impact of Seawater on the Production of Soil Water-Extractable Organic Carbon During Coastal Erosion," *Journal of Environmental Quality* 37 (2008): 2368–2374, https://doi.org/10.2134/jeq2007.0403.

25. J. Mitzscherling, M. Winkel, M. Winterfeld, et al., "The Development of Permafrost Bacterial Communities Under Submarine Conditions: Bacteria in Submarine Permafrost," *Journal of Geophysical Research: Biogeosciences* 122 (2017): 1689–1704, https://doi.org/10.1002/2017JG003859.

26. W. R. Eisner, J. G. Bockheim, K. M. Hinkel, et al., "Paleoenvironmental Analyses of an Organic Deposit From an Erosional Landscape Remnant, Arctic Coastal Plain of Alaska," *Palaeogeography, Palaeoclimatology, Palaeoecology* 217 (2005): 187–204, https://doi.org/10.1016/j.palaeo.2004.11.025.

27. S. Holm, J. Walz, F. Horn, et al., "Methanogenic Response to Long-Term Permafrost Thaw Is Determined by Paleoenvironment," *FEMS Microbiology Ecology* 96 (2020): fiaa021, https://doi.org/10.1093/femsec/fiaa021.

28. R. C. Frohn, K. M. Hinkel, and W. R. Eisner, "Satellite Remote Sensing Classification of Thaw Lakes and Drained Thaw Lake Basins on the North Slope of Alaska," *Remote Sensing of Environment* 97 (2005): 116–126, https://doi.org/10.1016/j.rse.2005.04.022.

29. M. J. Lara, A. D. McGuire, E. S. Euskirchen, et al., "Polygonal Tundra Geomorphological Change in Response to Warming Alters Future CO_2 and CH_4 Flux on the Barrow Peninsula," *Global Change Biology* 21 (2015): 1634–1651, https://doi.org/10.1111/gcb.12757.

30. Alaska Climate Research Center. 2023. "Climate Data for Utqiakvik. Periode: 1991–2020," https://akclimate.org/data/data-portal/.

31. J. Wolter, B. M. Jones, M. Fuchs, et al., "Post-Drainage Vegetation, Microtopography and Organic Matter in Arctic Drained Lake Basins," *Environmental Research Letters* 19 (2024): 045001.

32. Y. Jin, M. Chen, H. Yan, T. Wang, and J. Yang, "Sea Level Variation in the Arctic Ocean Since 1979 Based on ORAS5 Data," *Frontiers in Marine Science* 10 (2023): 1197456.

33. K. E. Nyland, N. I. Shiklomanov, D. A. Streletskiy, F. E. Nelson, A. E. Klene, and A. L. Kholodov, "Long-Term Circumpolar Active Layer Monitoring (CALM) Program Observations in Northern Alaskan Tundra," *Polar Geography* 44 (2021): 167–185.

34. F. Seemann, M. Jenrich, J. Lindemann, et al., "Sediment and Pore Water Investigations in Thermokarst Terrain Near Utqiagvik, Alaska [Dataset]," PANGAEA (2025), https://doi.org/10.1594/PANGAEA.974136.

35. G. Mollenhauer, H. Grotheer, T. Gentz, E. Bonk, and J. Hefter, "Standard Operation Procedures and Performance of the MICADAS Radiocarbon Laboratory at Alfred Wegener Institute (AWI), Germany," *Nuclear Instruments and Methods in Physics Research, Section B: Beam Interactions With Materials and Atoms* 496 (2021): 45–51.

36. P. J. Reimer, W. E. Austin, E. Bard, et al., "The IntCal20 Northern Hemisphere Radiocarbon Age Calibration Curve (0–55 Cal kBP)," *Radiocarbon* 62 (2020): 725–757.

37. M. Stuiver and P. J. Reimer, "Extended ^{14}C Data Base and Revised CALIB 3.0 14C Age Calibration Program," *Radiocarbon* 35 (1993): 215–230.

38. S. J. Blott and K. Pye, "GRADISTAT: A Grain Size Distribution and Statistics Package for the Analysis of Unconsolidated Sediments," *Earth Surface Processes and Landforms* 26 (2001): 1237–1248.

39. B. P. Koch, G. Kattner, M. Witt, and U. Passow, "Molecular Insights Into the Microbial Formation of Marine Dissolved Organic Matter: Recalcitrant or Labile?," *Biogeosciences* 11 (2014): 4173–4190, https://doi.org/10.5194/bg-11-4173-2014.

40. C. Guéguen, L. Guo, and N. Tanaka, "Distributions and Characteristics of Colored Dissolved Organic Matter in the Western Arctic Ocean," *Continental Shelf Research* 25 (2005): 1195–1207, https://doi.org/10.1016/j.csr.2005.01.005.

41. R Core Team. 2023. "R: A Language and Environment for Statistical Computing," R Foundation for Statistical Computing, Vienna, Austria, https://www.R-project.org/.

42. Posit team. 2023. "RStudio: Integrated Development Environment for R Posit Software, PBC Boston, MA," http://www.posit.co/.

43. G. P. Robertson, D. Coleman, C. Bledsoe, and P. Sollins, *Standard Soil Methods for Long-Term Ecological Research* (Oxford University Press, 1999).

44. M. L. Dolle, M. Laurent, J. Vollmer, and C. C. Treat, "Gas Production (CO_2 + CH_4) of an One Year Anaerobic Incubation With Salt Water From Two Permafrost Cores Near Utqiagvik, Alaska [Dataset]," PANGAEA (2024), https://doi.org/10.1594/PANGAEA.969148.

45. B. M. Jones, M. Z. Kanevskiy, A. D. Parsekian, et al., "Rapid Saline Permafrost Thaw Below a Shallow Thermokarst Lake in Arctic Alaska," *Geophysical Research Letters* 50, no. 22 (2023): e2023GL105552, https://doi.org/10.1029/2023GL105552.

46. J. Bockheim and K. Hinkel, "Characteristics and Significance of the Transition Zone in Drained Thaw-Lake Basins of the Arctic Coastal Plain, Alaska," *Arctic* (2005): 406–417.

47. E. M. Bristol, C. T. Connolly, T. D. Lorenson, et al., "Geochemistry of Coastal Permafrost and Erosion-Driven Organic Matter Fluxes to the Beaufort Sea Near Drew Point, Alaska," *Frontiers in Earth Science* 8 (2021): 598933, https://doi.org/10.3389/feart.2020.598933.

48. K. D. Johnson, J. Harden, A. D. McGuire, et al., "Soil Carbon Distribution in Alaska in Relation to Soil-Forming Factors," *Geoderma* 167 (2011): 71–84.

49. T. Roy Chowdhury, E. M. Herndon, T. J. Phelps, et al., "Stoichiometry and Temperature Sensitivity of Methanogenesis and CO_2 Production From Saturated Polygonal Tundra in Barrow, Alaska," *Global Change Biology* 21 (2015): 722–737, https://doi.org/10.1111/gcb.12762.

50. M. P. Waldrop, C. L. Chabot, S. Liebner, et al., "Permafrost Microbial Communities and Functional Genes Are Structured by Latitudinal and Soil Geochemical Gradients," *ISME Journal* 17 (2023): 1224–1235, https://doi.org/10.1038/s41396-023-01429-6.

51. L. L. Lapham, S. R. Dallimore, C. Magen, et al., "Microbial Greenhouse Gas Dynamics Associated With Warming Coastal Permafrost, Western Canadian Arctic," *Frontiers in Earth Science* 8 (2020): 15.

52. C. Schädel, E. A. G. Schuur, R. Bracho, et al., "Circumpolar Assessment of Permafrost C Quality and Its Vulnerability Over Time Using Long-Term Incubation Data," *Global Change Biology* 20 (2014): 641–652, https://doi.org/10.1111/gcb.12417.

53. T. W. Drake, K. P. Wickland, R. G. M. Spencer, D. M. McKnight, and R. Striegl, "G.: Ancient Low–Molecular-Weight Organic Acids in Permafrost Fuel Rapid Carbon Dioxide Production Upon Thaw," *Proceedings of the National Academy of Sciences* 112 (2015): 13946–13951, https://doi.org/10.1073/pnas.1511705112.

54. J. E. Vonk, P. J. Mann, S. Davydov, et al., "High Biolability of Ancient Permafrost Carbon Upon Thaw," *Geophysical Research Letters* 40 (2013): 2689–2693, https://doi.org/10.1002/grl.50348.

55. C. Ping, J. Jastrow, M. Jorgenson, G. Michaelson, and Y. Shur, "Permafrost Soils and Carbon Cycling," *Soil* 1 (2015): 147–171.

56. E. A. G. Schuur, J. Bockheim, J. G. Canadell, et al., "Vulnerability of Permafrost Carbon to Climate Change: Implications for the Global Carbon Cycle," *Bioscience* 58 (2008): 701–714, https://doi.org/10.1641/B580807.

57. L. D. A. Galera, T. Eckhardt, C. Beer, E. Pfeiffer, and C. Knoblauch, "Ratio of In Situ CO_2 to CH_4 Production and Its Environmental Controls in Polygonal Tundra Soils of Samoylov Island, Northeastern Siberia," *Journal of Geophysical Research: Biogeosciences* 128 (2023): e2022JG006956, https://doi.org/10.1029/2022JG006956.

58. K. Koch, C. Knoblauch, and D. Wagner, "Methanogenic Community Composition and Anaerobic Carbon Turnover in Submarine Permafrost Sediments of the Siberian Laptev Sea," *Environmental Microbiology* 11 (2009): 657–668, https://doi.org/10.1111/j.1462-2920.2008.01836.x.

59. C. N. Gutekunst, S. Liebner, A.-K. Jenner, et al., "Effects of Brackish Water Inflow on Methane-Cycling Microbial Communities in a Freshwater Rewetted Coastal Fen," *Biogeosciences* 19 (2022): 3625–3648, https://doi.org/10.5194/bg-19-3625-2022.

60. A. Söllinger and T. Urich, "Methylotrophic Methanogens Everywhere—Physiology and Ecology of Novel Players in Global Methane Cycling," *Biochemical Society Transactions* 47 (2019): 1895–1907.

61. G. Tanski, L. Bröder, D. Wagner, et al., "Permafrost Carbon and CO_2 Pathways Differ at Contrasting Coastal Erosion Sites in the Canadian Arctic, Frontiers," *Earth Science* 9 (2021): 630493, https://doi.org/10.3389/feart.2021.630493.

62. T. RoyChowdhury, L. Bramer, D. W. Hoyt, et al., "Temporal Dynamics of CO_2 and CH_4 Loss Potentials in Response to Rapid Hydrological Shifts in Tidal Freshwater Wetland Soils," *Ecological Engineering* 114 (2018): 104–114, https://doi.org/10.1016/j.ecoleng.2017.06.041.

63. J. E. Zlamal, T. K. Raab, M. Little, R. A. Edwards, and D. A. Lipson, "Biological Chlorine Cycling in the Arctic Coastal Plain," *Biogeochemistry* 134 (2017): 243–260.

64. N. D. Gray, C. M. McCann, B. Christgen, S. Z. Ahammad, J. A. Roberts, and D. W. Graham, "Soil Geochemistry Confines Microbial Abundances Across an Arctic Landscape; Implications for Net Carbon Exchange With the Atmosphere," *Biogeochemistry* 120 (2014): 307–317, https://doi.org/10.1007/s10533-014-9997-7.

65. R. Wagner, D. Zona, W. Oechel, and D. Lipson, "Microbial Community Structure and Soil pH Correspond to Methane Production in Arctic Alaska Soils," *Environmental Microbiology* 19 (2017): 3398–3410, https://doi.org/10.1111/1462-2920.13854.

66. Z. Wang, R. Delaune, W. Patrick, Jr., and P. Masscheleyn, "Soil Redox and pH Effects on Methane Production in a Flooded Rice Soil," *Soil Science Society of America Journal* 57 (1993): 382–385.

67. M. Deppe, K.-H. Knorr, D. M. McKnight, and C. Blodau, "Effects of Short-Term Drying and Irrigation on CO_2 and CH_4 Production and Emission From Mesocosms of a Northern Bog and an Alpine Fen," *Biogeochemistry* 100 (2010): 89–103.

68. D.-G. Kim, R. Vargas, B. Bond-Lamberty, and M. Turetsky, "Effects of Soil Rewetting and Thawing on Soil Gas Fluxes: A Review of Current Literature and Suggestions for Future Research," *Biogeosciences* 9 (2012): 2459–2483.

69. I. Kurganova, R. Teepe, and N. Loftfield, "Influence of Freeze-Thaw Events on Carbon Dioxide Emission From Soils at Different Moisture and Land Use," *Carbon Balance and Management* 2 (2007): 1–9.

70. P. Grogan, A. Michelsen, P. Ambus, and S. Jonasson, "Freeze–Thaw Regime Effects on Carbon and Nitrogen Dynamics in Sub-Arctic Heath Tundra Mesocosms," *Soil Biology and Biochemistry* 36 (2004): 641–654.

71. M. Van Gestel, R. Merckx, and K. Vlassak, "Microbial Biomass Responses to Soil Drying and Rewetting: The Fate of Fast- and Slow-Growing Microorganisms in Soils From Different Climates," *Soil Biology and Biochemistry* 25 (1993): 109–123.

72. K. Jentzsch, E. Männistö, M. E. Marushchak, et al., "Seasonal Controls on Methane Flux Components in a Boreal Peatland–Combining Plant Removal and Stable Isotope Analyses," *EGUsphere* 2024 (2024): 1–32.

73. J. A. Rosentreter, G. G. Laruelle, H. W. Bange, et al., "Coastal Vegetation and Estuaries Are Collectively a Greenhouse Gas Sink," *Nature Climate Change* 13 (2023): 579–587.

74. A. E. E. De Jong, M. H. In'T Zandt, O. H. Meisel, et al., "Increases in Temperature and Nutrient Availability Positively Affect Methane-Cycling Microorganisms in Arctic Thermokarst Lake Sediments," *Environmental Microbiology* 20 (2018): 4314–4327, https://doi.org/10.1111/1462-2920.14345.

75. N. Lotem, A. Pellerin, K. W. Anthony, A. Gafni, V. Boyko, and O. Sivan, "Anaerobic Oxidation of Methane Does Not Attenuate Methane Emissions From Thermokarst Lakes," *Limnology and Oceanography* 68 (2023): lno.12349, https://doi.org/10.1002/lno.12349.

76. C. Uhlig, J. B. Kirkpatrick, S. D'Hondt, and B. Loose, "Methane-Oxidizing Seawater Microbial Communities From an Arctic Shelf," *Biogeosciences* 15 (2018): 3311–3329, https://doi.org/10.5194/bg-15-3311-2018.

77. C. C. Treat, W. M. Wollheim, R. K. Varner, A. S. Grandy, J. Talbot, and S. Frolking, "Temperature and Peat Type Control CO_2 and CH_4 Production in Alaskan Permafrost Peats," *Global Change Biology* 20 (2014): 2674–2686, https://doi.org/10.1111/gcb.12572.

78. D. Zona, W. Oechel, J. Kochendorfer, et al., "Methane Fluxes During the Initiation of a Large-Scale Water Table Manipulation Experiment

in the Alaskan Arctic Tundra," *Global Biogeochemical Cycles* 23, no. 2 (2009): 1–11.

79. J. P. Schimel and C. Mikan, "Changing Microbial Substrate Use in Arctic Tundra Soils Through a Freeze-Thaw Cycle," *Soil Biology and Biochemistry* 37 (2005): 1411–1418, https://doi.org/10.1016/j.soilbio.2004.12.011.

80. S. B. Hodgkins, J. P. Chanton, L. C. Langford, et al., "Soil Incubations Reproduce Field Methane Dynamics in a Subarctic Wetland," *Biogeochemistry* 126 (2015): 241–249, https://doi.org/10.1007/s10533-015-0142-z.

81. R. M. Wilson, A. A. Zayed, K. B. Crossen, et al., "IsoGenie Project Coordinators, and IsoGenie Project Field Team: Functional Capacities of Microbial Communities to Carry Out Large Scale Geochemical Processes Are Maintained During Ex Situ Anaerobic Incubation," *PLoS ONE* 16 (2021): e0245857, https://doi.org/10.1371/journal.pone.0245857.

Supporting Information

Additional supporting information can be found online in the Supporting Information section. **Table S1:** Salt addition for brackish and sea water treatment. Chemical composition according to Koch et al. (2014). **Table S2:** Radiocarbon dating (14C ages [cal year BP]) for the UL and DLB site. Note plant species used for 14C dating were not identified. **Figure S1:** Core description of the Drained Lake Basin core and the Upland cores. Colors indicate different soil horizons. Layers of the same color indicate similar soil horizons. **Figure S2:** Overview of the incubation structure for each core. For clarity, the schematic displays the number of vials incubated for a single core only. Created in BioRender.com. **Figure S3:** Cumulative CO2 and CH4 production on carbon basis at the upland site (left) and drained lake basin (right) in AL1, AL2, PF1, and PF2 under the control treatment. Points represent the median production over four replicates. Please note the different y-axis scales. **Figure S4:** Cumulative CO2 production on a dry weight (left) and carbon basis (right) in non-surface layers at the upland site under the salt-less control treatment. Layers deeper than 74 cm are considered permafrost. Points represent the median production over four replicates. **Figure S5:** Cumulative CO2 production on a dry weight basis at the upland site (left) and drained lake basin site (right) under all treatments. Points represent the median production over four replicates. Please note the different y-axis scales. **Figure S6:** Cumulative CH4 production on a dry weight basis at the upland site (left) and drained lake basin site (right) under all treatments. Points represent the median production over four replicates. Please note the different y-axis scales.